Journal of Alloys and Compounds 509 (2011) 266–270

Contents lists available at ScienceDirect

Journal of Alloys and Compounds

journal homepage: www.elsevier.com/locate/jallcom

Correlation between the surface state and optical properties of S_6 site and C_2 site in nanocrystalline Eu^{3+}:Y_2O_3

Mingzhu Yang[a], Yu Sui[a,b,*], Shipeng Wang[a], Xianjie Wang[a], Yang Wang[a], Shuchen Lü[c], Tianquan Lü[a], Wanfa Liu[d]

[a] Center for Condensed Matter Science and Technology (CCMST), Department of Physics, Harbin Institute of Technology, Harbin 150001, People's Republic of China
[b] International Center for Materials Physics, Academia Sinica, Shenyang 110015, People's Republic of China
[c] Department of Physics, Harbin Normal University, Harbin 150001, People's Republic of China
[d] Dalian Institute of Chemical Physics, Dalian 116023, People's Republic of China

ARTICLE INFO

Article history:
Received 27 April 2010
Received in revised form 9 July 2010
Accepted 9 July 2010
Available online 16 July 2010

Keywords:
Luminescence
Hydrothermal method
Nanocrystals
Optical properties

ABSTRACT

Eu^{3+} doped Y_2O_3 nanocrystals are synthesized via precipitation and hydrothermal methods. With the increase of hydrothermal temperature, the number of surface states decreases when nanorods are formed. The decrease of surface states induces the increase in the ratio of S_6 site to C_2 site, and meanwhile results in the spectral red-shift of charge transfer band as well as the enhancement of red emission. The results indicate that the surface states and optical properties have close correlations.

1. Introduction

One-dimensional (1D) nanostructures, including nanorods, nanowires, nanofibers, and nanotubes, have attracted extensive interest over the past decades due to their potential application in a wide field [1–3]. Among all the nanostructures, rare-earth (RE) compounds have been extensively used in the fields of high-performance luminescent devices, magnets, catalysts, and other functional materials. These properties depend strongly on the composition and structure of materials. Recently, the synthesis and luminescence properties of RE ion doped 1D devices have attracted considerable attention [4–6].

As the main red emitting materials in commercial application on fluorescent lighting and display, Eu^{3+}:Y_2O_3 has attracted much attention [7,8]. It is well known that Eu^{3+}:Y_2O_3 absorbs ultraviolet (UV) light through the charge transfer band (CTB) and then yields red emission peaking around 610 nm. There exist two types of crystallographic sites in cubic Y_2O_3, S_6 site and C_2 site. The S_6 site is centrosymmetric in which electric dipole transition is forbidden, and only the *f–f* magnetic dipole transitions can be expected, so the S_6 site contributes little to the red emission. The C_2 site makes dominant contribution to the red emission around 610 nm which corresponds to $^5D_0$–$^7F_2$ transition of Eu^{3+} ion due to the absence of the centrosymmetric and the permission of electronic dipole transition. Hence, the observed CTB in the excitation spectra by monitoring $^5D_0$–$^7F_2$ transition is mainly from the Eu^{3+} ions at the C_2 site [9]. Although the S_6 site has little contribution to the red emission, it could still compete with the C_2 site for UV absorption. It has been reported in several publications that the two sites have a close relationship. One group reported that the efficient Eu^{3+} (S_6) → Eu^{3+} (C_2) energy transfer for higher concentrations of Eu^{3+} reduces the fraction of the Eu^{3+} (S_6) emission [10]. Another group has reported that comparing with the bulk counterpart, the ratio of the S_6 sites to the C_2 sites in nanocrystal decreases remarkably [5]. However, the correlation between the surface states and the optical properties of the two sites is still unclear. Eu^{3+}:Y_2O_3 nanocrystals exhibit a lot of special spectra properties with the increase of surface states [5,11,12]. For instance, it has been reported that UV light irradiation can induce spectral change depending on sample size in the CTB in Eu^{3+}:Y_2O_3 nanowires [5]; the morphology and shape of Eu^{3+}:Y_2O_3 nanocrystals can influence the luminescence efficiency of Eu^{3+} [11]; and the quenching concentration of Eu^{3+} much higher than that of micro-scaled powders [12]. So it is interesting to study the correlation between

* Corresponding author at: Center for Condensed Matter Science and Technology (CCMST), Department of Physics, Harbin Institute of Technology, Harbin 150001, People's Republic of China. Tel.: +86 45186418403.
E-mail address: suiyu@hit.edu.cn (Y. Sui).

0925-8388/$ – see front matter © 2010 Elsevier B.V. All rights reserved.
doi:10.1016/j.jallcom.2010.07.088

the surface states and the optical properties of the two sites in nanocrystals.

In this study, we report the preparation of Eu^{3+} doped Y_2O_3 nanocrystals through a facile hydrothermal process without using any catalyst or template followed by subsequent heat treatment process in air. We discuss the correlation between the surface states and the optical properties of the Eu^{3+} doped Y_2O_3 nanocrystals. The excitation spectra of the CTB for Eu^{3+} at the S_6 site are investigated in Eu^{3+} doped Y_2O_3 nanocrystals. The decomposition of excitation spectra shows that the ratio of S_6 sites to C_2 sites increases with the decrease of surface states. In addition, both CTB of S_6 site and C_2 site exhibit red-shift accompanied with the red emission enhancement when the surface states are decreased. These results can shed light on the investigation of the influence of the surface states on the luminescence property of nanocrystals.

2. Experimental

5 mol% of Eu^{3+} doped Y_2O_3 (Eu^{3+}:Y_2O_3) nanocrystals were prepared by precipitation method and hydrothermal treatment. Stoichiometric high-purity Y_2O_3 and Eu_2O_3 were dissolved in HNO_3 first. Then the final pH value was adjusted with NaOH solution. After being stirred for 1 h, a milky colloid solution was obtained. For precipitation method, the precipitate was washed with deionized water for several times and then dried at 60 °C. For hydrothermal treatment, the milky colloid solution was transferred into Teflon-lined autoclaves to be treated by hydrothermal method. In order to obtain nanocrystals with different morphologies, the milky colloid solutions were subsequently heated at 120–180 °C for 12 h. The obtained suspension was cooled to room temperature naturally and the precipitate was washed with deionized water several times and then dried at 60 °C. Finally, the obtained Eu^{3+}:$Y(OH)_3$ powder prepared by precipitation method and hydrothermal treatment were converted into Eu^{3+}:Y_2O_3 powder by annealing at 500 °C for 3 h in air. The XRD data of the specimens were recorded by a Rigaku D/max-γB diffractometer using Cu Kα radiation (λ = 0.15418 nm). The luminescence measurements were performed on Hitachi F-4500 Fluorescence Spectrophotometer at room temperature. The morphology of the samples was determined by the transmission electron microscope (TEM), Philips CM12. The infrared absorption spectra were recorded with an IFS66V/S Fourier transform infrared spectrometer. Decay profiles were measured by a spectrometer (Bruker Optics 250IS/SM) coupled with an intensified charge coupled device detector (IStar740, Andor)

3. Results and discussion

Fig. 1 displays the XRD patterns of Eu^{3+}:Y_2O_3 powders prepared at different conditions. The XRD data confirm that all the samples are assigned to be single-phase of the cubic structure (JPDS No. 86-1107) with a lattice constant of 10.602 Å. One can find that the FWHM of the peaks in XRD patterns becomes narrower with increasing hydrothermal temperature, indicating that the crystallinity of Eu^{3+}:Y_2O_3 enhances at higher hydrothermal temperatures.

Fig. 2 shows the TEM images of Eu^{3+}:Y_2O_3 nanocrystals. Under precipitation condition, the morphology of Eu^{3+}:Y_2O_3 nanocrystals is nanosheets, and their side length is about 170 nm (Fig. 2a). When the hydrothermal temperature is 120 °C, some 1D nanorods appear among the nanosheets (Fig. 2b). When the temperature increases to 160 °C, the amount of nanosheets decreases to only a small portion (Fig. 2c). Only 1D nanorods are present in the sample with a diameter about 130 nm and a length about 1.7 μm after the reaction temperature increases to 180 °C (Fig. 2d). From the XRD results, we can see that the crystallization is improved with the increase of reaction temperature. Moreover, the specific surface area of the nanocrystals decreases when the morphology changes from nanosheets to nanorods (Fig. 2), and the surface states decrease with the improved crystallization and decreased specific surface area. The change of surface states with different morphologies would influence the luminescence properties of Eu^{3+}:Y_2O_3 nanocrystals.

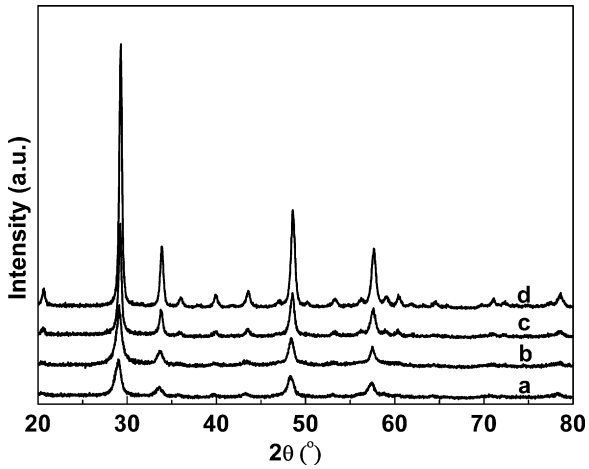

Fig. 1. XRD patterns of Eu^{3+}:Y_2O_3 nanocrystals corresponding to different synthesis conditions: (a) precipitation method, (b) 120 °C and 12 h, (c) 160 °C and 12 h, and (d) 180 °C and 12 h.

Fig. 3 displays the excitation spectra of Eu^{3+}:Y_2O_3 nanocrystals. As shown in Fig. 3, the excitation spectra intensity of the sample prepared by hydrothermal reaction is enhanced corresponding to that of the samples synthesized under precipitation treatment, while the CTB of S_6 site cannot be observed in the sample obtained under lower reaction temperature. However, with the increase in hydrothermal reaction temperature, the excitation spectra can be decomposed into two Gaussian components. In the isostructural Y_2O_3 host, it is reported that the CTB of Eu^{3+} at S_6 site is positioned slightly higher than that of Eu^{3+} at C_2 site [13,14]. Therefore, we attribute the shorter wavelength component of CTB around 235 nm to Eu^{3+} at the S_6 site, and the other band occurring around 255 nm to Eu^{3+} at the C_2 site. By comparing the spectra of the samples synthesized with lower reaction temperature, an increase of the ratio of S_6 site to C_2 site in the decomposition of excitation spectra can be clearly observed with the increase of hydrothermal temperature (see Table 1). These phenomena are believed to be associated with the surface states of the nanocrystals [5]. The local symmetry at several layers of the samples lowers when they are synthesized under lower temperature, namely, more Eu^{3+} ions locate in or near the particle surface where there exists a large number of surface states, i.e. dangling bonds and disorder structures. With the increase of hydrothermal temperature, the surface states decrease, inducing the decrease of lattice distortion, so it is easy to observe the CTB of Eu^{3+} at the centrosymmetric S_6 site in the nanocrystals.

It is also shown in Fig. 3 that CTBs of Eu^{3+} at both S_6 and C_2 sites exhibit a red-shift with the increases of reaction temperature (see Table 1), which can be attributed to the shorten of Eu–O distance in these samples [15]. With the decrease of reaction temperature, the proportion of the atoms at surface layers increases with grain size decreasing. The increase of the ratio of surface atoms results in an

Table 1
The lattice constant, intensity ratio of S_6/C_2 sites as well as the peak position of S_6 site and C_2 site in Eu^{3+}:Y_2O_3 nanocrystals.

Synthesis conditions	Lattice constant (Å)	Intensity ratio of S_6/C_2 sites	Peak position of S_6 site (nm)	Peak position of C_2 site (nm)
Precipitation	10.621	–	–	249.6
12 h 120 °C	10.619	–	–	249.7
12 h 160 °C	10.608	0.82	234.4	251.2
12 h 180 °C	10.601	0.90	235.9	254.2

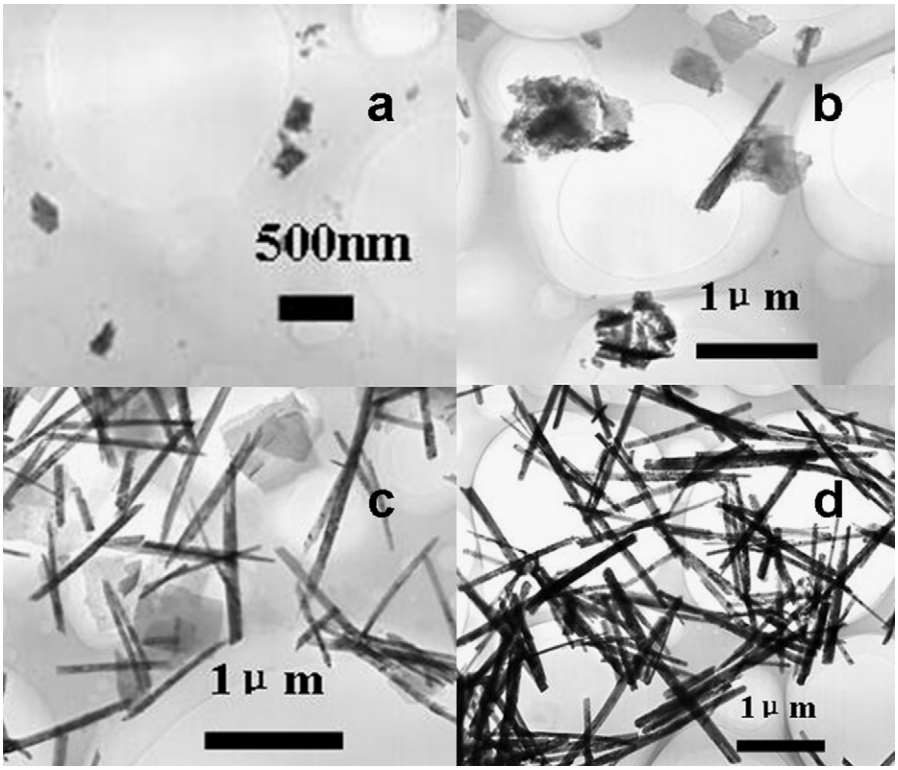

Fig. 2. TEM images of Eu^{3+}:Y_2O_3 nanocrystals corresponding to different synthesis conditions: (a) precipitation method, (b) 120 °C and 12 h, (c) 160 °C and 12 h, and (d) 180 °C and 12 h.

increased number of broken Y–O bond at the surface. The unpaired electronic orbitals at the surface repel each other and result in larger values of equilibrium lattice parameters [16,17]. The increase in the proportion of surface atoms enhances the proportion of local displacement, and hence, results in the increases of the overall lattice distortion, finally changes the lattice constant [15].

As shown in Table 1, the lattice constant of Eu^{3+}:Y_2O_3 increases with the decrease of reaction temperature. Since the crystal structure of Eu^{3+}:Y_2O_3 is cubic, the average the bond distance varies directly as the lattice constant. A longer bond distance represents a higher ionicity [18], whereas the shorter bond distance represents a higher covalency [15]. The decrease in the lattice constant for nanocrystals, synthesized under increasing reaction temperature (Table 1), means the increase in covalency. The CTB of Eu^{3+}:Y_2O_3 corresponds to the electronic transition from the 2*p* orbital of O^{2-} to the 4*f* orbital of Eu^{3+}, which is related closely to the covalency between O^{2-} and Eu^{3+}. The enhancement of covalency can result in the decrease in energy for electron transfer from O^{2-} to Eu^{3+} [15,19]. Consequently, the decrease of surface distortion induces the decrease in lattice constant and increase in covalency, and then a red-shift of CTB is observed.

As mentioned above, the C_2 site performs the dominant contribution to the 610 nm emission, so usually the decrease of C_2 site leads to the decrease of red emission. However, in this case it is interesting to note the emission intensity of 610 nm enhances when the ratio of S_6 site to C_2 site increases (Fig. 4). The increase

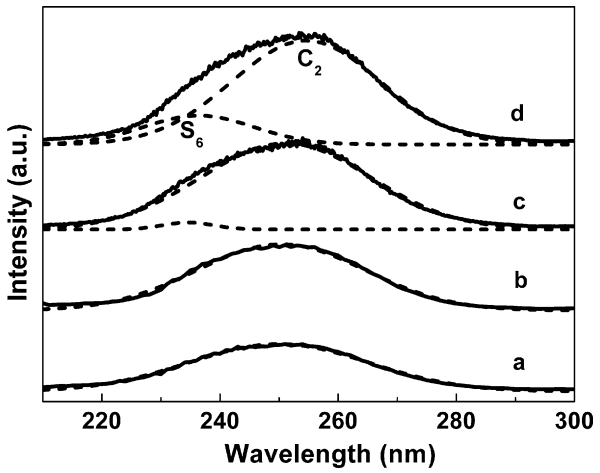

Fig. 3. Excitation spectra of Eu^{3+}:Y_2O_3 nanocrystals corresponding to different synthesis conditions: (a) precipitation method, (b) 120 °C and 12 h, (c) 160 °C and 12 h, and (d) 180 °C and 12 h.

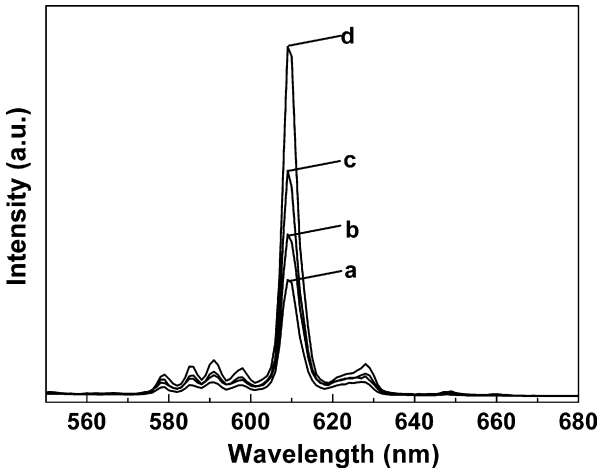

Fig. 4. Emission spectra of Eu^{3+}:Y_2O_3 nanocrystals corresponding to different synthesis conditions: (a) precipitation method, (b) 120 °C and 12 h, (c) 160 °C and 12 h, and (d) 180 °C and 12 h.

in emission intensity of C_2 site results from the enhanced luminescence efficiency principally governed by the nonradiative process of host materials. The multiphonon nonradiative decay rate can be expressed by the following energy gap law [20]:

$$W_n = W_0\left[1 - \exp\left(-\frac{h\nu}{kT}\right)\right]^{-n} \quad (1)$$

where W_n is the rate at temperature T, W_0 is the rate at 0 K, and $n = \Delta E/h\nu$ in which ΔE is the energy gap between the levels involved whereas ν is the relevant phonon frequency. As ΔE is equal to or less than 4–5 times the high-energy phonons, the multiphonon nonradiative relaxation can be competitive with the radiative processes. Atomic groups with higher vibrational frequency will increase the nonradiative relaxation rate and hence decrease luminescence efficiency [20]. To obtain high luminescence efficiency, atomic groups with high vibrational frequency must be removed from a system.

Fig. 5 presents the FT-IR transmission spectra of Eu^{3+}:Y_2O_3 nanocrystals. The absorption bands of OH^- (around 3400 cm^{-1}) and CO_3^{2-} groups (around 1500 cm^{-1}) become weaker gradually with increasing synthesis temperature. There are fewer OH^- or CO_3^{2-} groups in the Eu^{3+}:Y_2O_3 nanocrystals synthesized at 180 °C and 12 h, so this sample has higher luminescence efficiency and exhibiting stronger emission intensity (Fig. 4). By contrast, the samples of Eu^{3+}:Y_2O_3 nanocrystals synthesized at lower temperatures exhibit relatively weak luminescence, which can be attributed to luminescence quenching via nonradiative energy transfer to OH^- or CO_3^{2-} groups.

In order to verify that the enhancement of luminescence intensity comes from the decrease of nonradiative transition process, we investigated the decay behavior of 610 nm emission of Eu^{3+}:Y_2O_3 nanocrystals (Fig. 6). The fluorescence decay curves can all be fitted

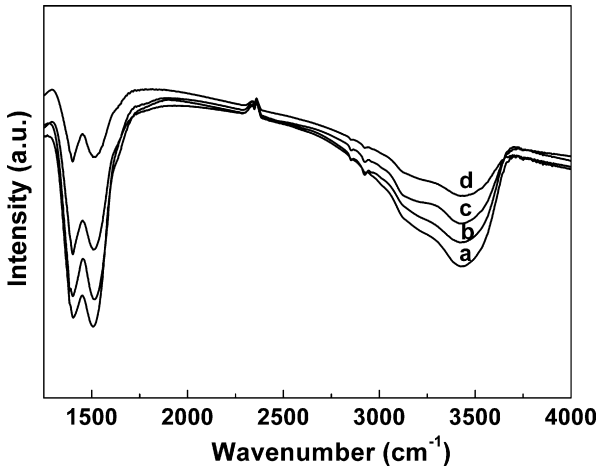

Fig. 5. FT-IR spectra of Eu^{3+}:Y_2O_3 nanocrystals corresponding to different synthesis conditions: (a) precipitation method, (b) 120 °C and 12 h, (c) 160 °C and 12 h, and (d) 180 °C and 12 h.

to single exponentials according to Eq. (2) [21],

$$I = A\exp\left(-\frac{t}{\tau}\right) + B \quad (2)$$

where τ is the fluorescence lifetime, t is the delay time, I is the relative intensity, and A and B are the constants. The fitting results show that, with the increase of hydrothermal reaction temperature, the fluorescence lifetime increases from 1.16 ms to 1.81 ms. It is well understood that the reverse of the lifetime equals to the sum of the radiative transition and nonradiative relaxation rates. The increase of fluorescence lifetimes suggests that more defect states on the surface of the sample would lead to substantially increased nonradiative relaxation rates and shortened lifetimes of Eu^{3+} emission

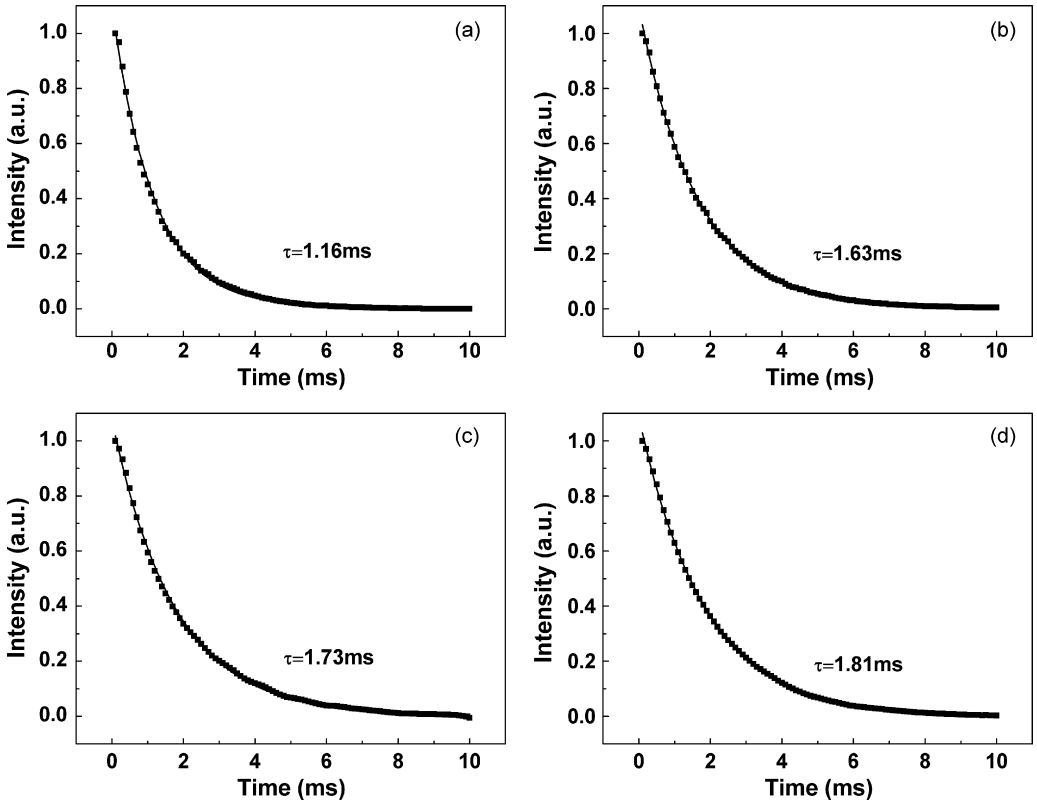

Fig. 6. Fluorescence decay curves for the 610 nm emission of Eu^{3+}:Y_2O_3 nanocrystals corresponding to different synthesis conditions: (a) precipitation method, (b) 120 °C and 12 h, (c) 160 °C and 12 h, and (d) 180 °C and 12 h.

[22,23]. Thus, we can conclude that the significantly different intensities of the 610 nm emissions are largely dependent on surface states of the Eu^{3+}:Y_2O_3 nanocrystals.

4. Conclusions

In conclusion, the decreased surface states decrease the lattice distortion and shorten the lattice constant. Such change in lattice constant increases the covalency of Eu–O bonds and thus shifts the CTB toward the lower-energy side. The reduced surface states enhance the local symmetry of the samples and then increase the ratio of S_6 sites to C_2 sites, and meanwhile the decrease of surface states lessens the nonradiative process, which increases the red emission intensity finally.

Acknowledgments

This work was supported by the National Natural Science Foundation of China (Grant Nos. 50672019 and 10804024) and the Scientific Research Foundation for the Returned Overseas Chinese Scholars, State Education Ministry and supported by "the Fundamental Research Funds for the Central Universities" (Grant No. HIT.NSRIF.2009056).

References

[1] Y.N. Xia, P.D. Yang, Y.G. Sun, Y.Y. Wu, B. Mayers, B. Gates, Y.D. Yin, F. Kim, H.Q. Yan, Adv. Mater. 15 (2003) 353.
[2] E. Bacaksiz, G. Cankaya, I. Polat, S. Yilmaz, C. Duran, M. Altunbas, J Alloys Compd. 496 (2010) 560.
[3] T. Kijima, T. Isayama, M. Sekita, M. Uota, G. Sakai, J Alloys Compd. 485 (2009) 730.
[4] Y.B. Mao, J.Y. Huang, R. Ostroumov, K.L. Wang, J.P. Chang, J. Phys. Chem. C 112 (2008) 2278.
[5] Y. Li, J. Zhang, X. Zhang, Y. Luo, S. Lu, Z. Hao, X.J. Wang, J. Phys. Chem. C 113 (2009) 17705.
[6] Z. Xu, J. Yang, Z. Hou, C. Li, C. Zhang, S. Huang, J. Lin, Mater. Res. Bull. 44 (2009) 1850.
[7] G. Dong, Y. Chi, X. Xiao, X. Liu, B. Qian, Z. Ma, E. Wu, H. Zeng, D. Chen, J. Qiu, Opt. Express 17 (2009) 22514.
[8] S. Zhong, S. Wang, Q. Liu, Y. Wang, S. Wang, J. Chen, R. Xu, L. Luo, Mater. Res. Bull. 44 (2009) 2201.
[9] M. Jia, J. Zhang, S. Lu, J. Sun, Y. Luo, X. Ren, H. Song, X. Wang, Chem. Phys. Lett. 384 (2004) 193.
[10] E. Zych, J. Phys.: Condens. Matter 14 (2002) 5637.
[11] X.R. Hou, S.M. Zhou, Y.K. Li, W.J. Li, J. Alloys Compd. 494 (2010) 382.
[12] R. Srinivasan, N. Rajeswari Yogamalar, J. Elanchezhiyan, R. Justin Joseyphus, A. Chandra Bose, J Alloys Compd. 496 (2010) 472.
[13] C.N. Wang, W.P. Zhang, M.J. Yin, J. Alloys Compd. 474 (2009) 180.
[14] Z.F. Wang, W.P. Zhang, L. Lin, B.G. You, Y.B. Fu, M. Yin, Opt. Mater. 30 (2008) 1484.
[15] T. Igarashi, M. Ihara, T. Kusunoki, K. Ohno, T. Isobe, M. Senna, Appl. Phys. Lett. 76 (2000) 1549.
[16] P. Ayyub, V.R. Palkar, S. Chattopadhyay, M. Multani, Phys. Rev. B 51 (1995) 6135.
[17] S. Roy, I. Dubenko, D.D. Edorh, N. Ali, J. Appl. Phys. 96 (2004) 1202.
[18] D.F. Shriver, P.W. Atkins, C.H. Langford, Inorganic Chemistry, Oxford University Press, Oxford, 1990.
[19] Z.W. Pei, Q. Su, S.H. Li, J. Lumin. 50 (1991) 123.
[20] H. Guo, N. Dong, M. Yin, W.P. Zhang, L.R. Lou, S.D. Xia, J. Phys. Chem. B 108 (2004) 19205.
[21] Q. Zhu, J.G. Li, X.D. Li, X.D. Sun, Acta Mater. 57 (2009) 5975.
[22] Q.L. Dai, H.W. Song, M.Y. Wang, X. Bai, B. Dong, R.F. Qin, J. Phys. Chem. C 112 (2008) 19399.
[23] H.W. Song, J.W. Wang, B.J. Chen, H.S. Peng, S.Z. Lu, Chem. Phys. Lett. 376 (2003) 1.